

Ballistic electron focusing by elliptic reflecting barriers

J. J. Heremans^{a)} and S. von Molnár

MARTECH, Florida State University, Tallahassee, Florida 32306-4000

D. D. Awschalom

Department of Physics, University of California, Santa Barbara, California 93106

A. C. Gossard

Department of Materials, University of California, Santa Barbara, California 93106

(Received 15 July 1998; accepted for publication 5 January 1999)

We investigate reflection of ballistic electrons off an elliptic barrier in a high quality AlGaAs/GaAs heterostructure. Electrons injected at one focal point of an ellipse are collected at the second focal point, or at the midpoint. Application of a magnetic field perpendicular to the plane of the ellipse modifies the focusing effects by distorting the electrons' paths, resulting in a novel four-terminal negative magnetoresistance phenomenon. Several secondary features in the magnetoresistance are observed and are interpreted in the light of numerical path simulations. © 1999 American Institute of Physics. [S0003-6951(99)03809-7]

The large carrier mean free path in two-dimensional electron systems (2DESs) at the AlGaAs/GaAs interface affords methods of controlling magnetoresistance characteristics. If the carrier mean free path is substantially larger than the length scale defined by the device geometry, the classical cyclotron orbit D_c —associated with an external field B —determines the scale for the spatial inhomogeneity of current and potential distributions. Varying D_c through the applied B results in magnetosize effects through the interaction between the device geometry and D_c . Adapting the device geometry to obtain desired magnetoresistance effects offers opportunities for the design of magnetic microsensors for high-density data storage. We present a class of geometries for control of ballistic electrons in mesoscopic structures, based on specular reflection from elliptic barriers. We demonstrate that electron focusing effects can be achieved without an external B , while application of B predictably modifies the response. The device combines two effects: (1) the geometrical property of conic sections, whereby rays emanating from one focal point, and reflecting from the conic section surface, are focused onto the second focal point, and (2) specular reflection of carriers impinging on a potential barrier. Specular reflection of ballistic carriers off a potential barrier is experimentally well established, from observation of transverse magnetic focusing (TMF), first achieved in Bi and other metals¹ and later in 2DESs² and two-dimensional hole systems.³ The connection between geometrical optics and ballistic electron transport was established by the lensing action from a patterned metal gate.⁴ Our use of reflective rather than refractive ‘‘optics’’ circumvents problems of homogeneity and reduced electron mean free path under the refractive gate.

The device is assembled from a TMF geometry¹⁻³ with the addition of a barrier, forming half an ellipse, straddling the injector and collector apertures. Figure 1 shows a photograph of the device, where three isolated apertures (a, b, c)

interrupt a continuous straight barrier. The two outer apertures (a, c) are positioned at the foci of the elliptic barrier, with aperture b in the middle. The elliptic and straight barriers are not joined, permitting a bias current to flow. Forcing a current between aperture a and a contact external to the geometry shown, injects carriers towards the elliptic barrier, wherefrom, after specular reflection, the carriers are focused onto either aperture c or b , inducing a voltage in the corresponding lead. The emphasis of the present work is the study of magnetic field induced deviations from straight carrier paths and the concomitant effect on the focusing properties of the ellipse.

The 2DES is contained in a δ -doped AlGaAs/GaAs heterostructure, with a distance of surface to 2DES of 800 Å. The straight and elliptic barriers were fabricated by electron beam lithography and wet etching.³ A gate was evaporated over the entire device, allowing the carrier density (and hence mobility and mean free path) to be optimized by varying the gate voltage. The mean free path for the conditions of Fig. 2 was 15 μm . The lithographic widths of apertures a, b , and c in Fig. 1 are 1.0 μm and the apertures are separated by 3.0 μm . The actual conducting width in the 2DES is smaller ($\sim 0.6 \mu\text{m}$), due to side etching and to the existence of an electrostatic depletion layer.⁵ We assume the width of the apertures to be large compared to the Fermi wavelength, al-

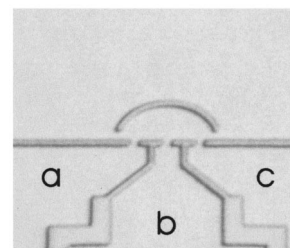


FIG. 1. Optical photograph of the device geometry. Three apertures, a, b , and c , allow injection or detection of carriers. Apertures a and c are located at the foci of the elliptic barrier, aperture b is located in the middle of a and c . The distance $a-c$ is 6.0 μm .

^{a)}Electronic mail: jean_heremans@emcore.com

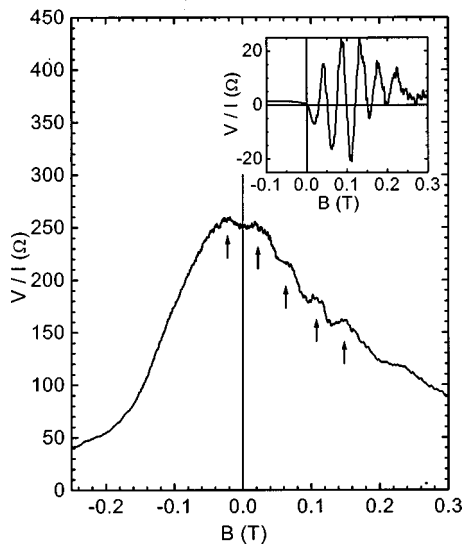


FIG. 2. Voltage measured at c with current injection at a vs magnetic field B (in a four-probe geometry; the other two contacts are external to and far away from the elliptic enclosure). The voltage is normalized to the injected current. Extrema discussed in the text are indicated by arrows ($T = 0.35$ K). Inset: voltage (normalized to injected current) vs magnetic field B measured in a TMF geometry without elliptic barrier. The distance between the current injection aperture and the voltage aperture for this device is $5.0 \mu\text{m}$ (electron mean free path $\approx 13 \mu\text{m}$; $T = 0.35$ K). TMF peaks appear at values of B where the cyclotron diameter fits an integer number of times between current injection and voltage measurement apertures.

lowing us to neglect the formation of one-dimensional subbands and coherent excitation of quantum-mechanical edge states.² The distance between the elliptic and straight barriers will vary slightly with the width of the depletion layer around the barriers. The focusing properties of the ellipse were designed assuming a depletion layer width of $\sim 0.2 \mu\text{m}$. The optical path length (reflecting once off the elliptic barrier) from a to c amounts to $9.0 \mu\text{m}$, independent of the starting angle of the path (a constant of the ellipse). Measurements were performed by lock-in detection at 0.35 K in a four-probe configuration.

Figure 2 shows the typical behavior versus B of the voltage registered between c and a contact external to the ellipse, upon injecting a current from a to a fourth contact (external to the ellipse as well). We have divided the measured voltage by the injected current, after ascertaining linearity. The trace closely obeys the Büttiker reciprocity relation on interchanging the current and voltage contacts and reversing the direction of B ,⁶ and was observed with only minor variations over a wide range of gate voltages, for several samples. The trace can be approached as a superposition of several magnetosize effects. First, as a main effect, the signal envelope decays rapidly away from $B = 0$ in either direction. We attribute this decay to a disruption of the focusing properties of the ellipse due to the magnetic field induced distortion of the electrons' paths. Second, however, the signal is not strictly maximal at $B = 0$, as this point is overshadowed by two peaks at small positive ($B \approx 0.020$ T) and negative ($B \approx -0.023$ T) values. Third, for $B > 0$ we recognize three TMF inflections ($B \approx 0.071, 0.112, 0.151$ T). These occur whenever the cyclotron orbit diameter D_c fits an integer number of times in the distance $a-c$.¹⁻³ The presence of a TMF signal attests to the ballistic nature of the electron transport as well as to the

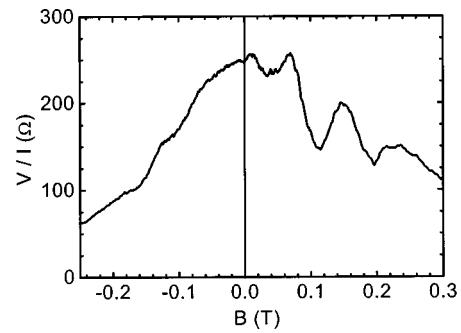


FIG. 3. Voltage (normalized to injected current) measured at b with current injection at a vs magnetic field B (four-probe geometry; $T = 0.35$ K).

reflectivity of the barrier. A strong reduction is noticed in the strength of the first TMF peak, expected to appear at $B \approx 0.038$ T. The inset to Fig. 2 shows a TMF spectrum recorded for a device similar to Fig. 1 but lacking the elliptic focusing barrier. Five clear peaks are visible, at the positions expected for this device. A comparison with the main panel is revealing: the background on which the TMF peaks ride is featureless and flat, especially for low B . Figure 3 contains the magnetoresistance recorded at the middle aperture b under the same conditions of current injection and gate voltage than the main panel in Fig. 2. Similarly to the signal at c , the envelope at b decays away from $B = 0$. The shorter distance ($3 \mu\text{m}$) between b and a accounts for an enhanced magnitude of the TMF peaks observed at 0.071 and 0.151 T. Despite the shorter distance $a-b$, the maxima at $B \approx 0.020$ and -0.023 T present in the main panel in Fig. 2 are absent. A small maximum instead appears at $B \approx 0.010$ T.

In the simplest picture, we expect the signal obtained at c upon injection from a to peak at $B = 0$, while the signal at b should not display this $B = 0$ maximum. However, depending on B and some device nonidealities, the elliptic geometry sustains several more complex focusing phenomena. While the main effect of B on the signal at c consists of a defocusing action, as we will describe below, some ballistic electron trajectories at specific values of B can lead to additional strong structure in the magnetoresistance. This is illustrated in Fig. 4. Panel I contains a semiclassical simulation of electron trajectories corresponding to $B = -0.023$ T (see Fig. 2). The elliptic barrier cleanly focuses electrons emanating from aperture a onto c , independently of the starting angle of the trajectory. Such operation is identical to TMF, and results in the maximum experimentally observed at this value of B . Only two reflections off the elliptic barrier are necessary. Trajectories involving a large number of reflections are damped by the imperfect specularity of the barrier, and suffer a decay exponential in the length of the path involved.³ Panel II shows trajectories for $B = 0.020$ T. Here only starting angles inclined toward c find a short path to c , other trajectories being scattered off course. Since only a fraction of electrons injected from a will contribute to a signal at c , the $B \approx 0.020$ T maximum in Fig. 2 is expected to be of lesser magnitude, as evidenced by the data. At low B the ellipse reflects the carriers toward c , even if (see, e.g., panel I) the trajectories are initially inclined away from c . This directional effect disappears when B is sufficiently large to deflect the injected carriers before they reach the elliptic barrier, and leads to the envelope observed in Fig. 2. Absence of this

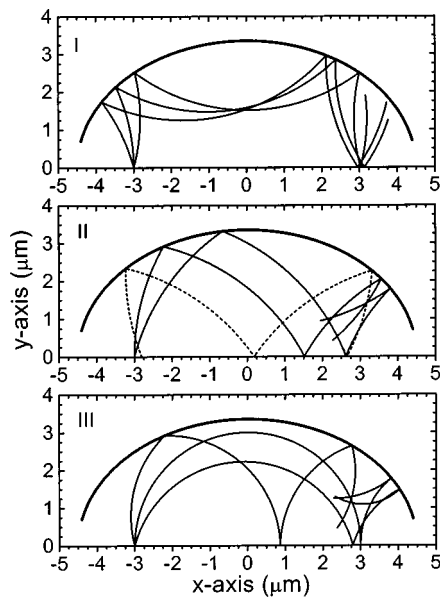


FIG. 4. Calculated electron trajectories corresponding to the extrema in Fig. 2. Panel I: $B = -0.023$ T; panel II: $B = 0.020$ T; panel III: $B = 0.038$ T (corresponding to the reduced first TMF peak).

action in the TMF geometry then leads to the absence in the inset in Fig. 2 of a similar broad maximum at $B = 0$. Superposition of the maxima at $B \approx 0.020$ and -0.023 T on the overall defocusing trend results in the low field behavior experimentally observed in Fig. 2. Panel III depicts trajectories for $B = 0.038$ T, corresponding to the first expected TMF peak. Starting angles inclined away from c do not contribute, and we believe this explains the lack of a clear first TMF peak in the data of Fig. 2. The remnants of a peak can still be discerned as a shoulder, obscured by the clearer maximum at $B \approx 0.020$ T. Trajectories corresponding to the small maximum observed at $B \approx 0.010$ T in Fig. 3 reveal that focusing can also occur towards aperture b . Apertures a and b have a finite width, and trajectories starting within the width of a can impinge within the width of b for a range of small positive fields around $B \approx 0.010$ T. The cyclotron orbit curvature at small positive fields causes the trajectories to fall short of c and thus to land closer to b (see, e.g., the dashed trajectory in panel II). Combined with the tendency of the elliptic barrier to deflect carriers in the direction of c , this explains the broad maximum culminating at $B \approx 0.010$ T in Fig. 3. Thus, focusing onto b can occur due to nonidealities in the geometry's definition.

Some important differences lie between this work and recent resistance measurements on ballistic cavities interpreted as weak localization phenomena.⁷ The scale of B over which the features in Fig. 2 occur preclude their interpretation in the light of weak localization. Using the full-width at half-maximum, ΔB_{FWHM} , of the envelope in Fig. 2 to calculate the diameter D_{WL} of the characteristic trajectory loop area A , by $\Delta B_{\text{FWHM}} = h/2\pi eA$,⁷ we find $D_{\text{WL}} \approx 60$ nm, an extremely small length compared to the ellipse dimensions, or even compared to the aperture width. The extreme length discrepancy necessitates the interpretation of Fig. 2 as a manifestation of classical trajectories. Finally, Ref. 7 describes two-contact conventional magnetoresistance measurements (symmetric in B), while our work presents four-contact nonlocal probing from inside a ballistic cavity (nonsymmetric in B).

In conclusion, we have analyzed the field-dependent behavior of an elliptic ballistic focusing device. A clear indication of focusing was detected in the rapid decay of the signal envelope on applying a perpendicular magnetic field. Robust structure superposed on this decay can be attributed to semiclassical electron trajectories that result in focusing action.

The authors thank T. Schultz and F. Sharifi for the use of the electron beam lithography equipment. This work was supported by NSF DMR 95-27553, 95-10518, and AFOSR F49620-96-0018.

¹V. S. Tsoi, JETP Lett. **19**, 70 (1974); V. S. Tsoi and I. I. Razgonov, JETP Lett. **25**, 26 (1977); P. A. M. Benistant, G. F. A. van de Walle, H. van Kempen, and P. Wyder, Phys. Rev. B **33**, 690 (1986).

²H. van Houten, C. W. J. Beenakker, J. G. Williamson, M. E. I. Broecker, P. H. M. van Loosdrecht, B. J. van Wees, J. E. Mooij, C. T. Foxon, and J. J. Harris, Phys. Rev. B **39**, 8556 (1989).

³J. J. Heremans, M. B. Santos, and M. Shayegan, Appl. Phys. Lett. **61**, 1652 (1992); J. J. Heremans, M. B. Santos, and M. Shayegan, Surf. Sci. **305**, 348 (1994).

⁴J. Spector, H. L. Stormer, K. W. Baldwin, L. N. Pfeiffer, and K. W. West, Appl. Phys. Lett. **56**, 1290 (1990); U. Sivan, M. Heiblum, and C. P. Umbach, Phys. Rev. Lett. **63**, 992 (1989).

⁵J. H. Davies, Semicond. Sci. Technol. **3**, 995 (1988); S. E. Laux, D. J. Frank, and F. Stern, Surf. Sci. **196**, 101 (1988).

⁶M. Büttiker, Phys. Rev. Lett. **57**, 1761 (1986).

⁷A. M. Chang, H. U. Baranger, L. N. Pfeiffer, and K. W. West, Phys. Rev. Lett. **73**, 2111 (1994); R. P. Taylor, R. Newbury, A. S. Sachrajda, Y. Feng, P. T. Coleridge, C. Dettmann, N. Zhu, H. Guo, A. Delage, P. J. Kelly, and Z. Wasilewski, Phys. Rev. Lett. **78**, 1952 (1997).